5. Results

5.1. ISOLATION AND CHARACTERIZATION OF MURINE MN/CA9 cDNA

5.1.1. Identification of Murine MN/CA9 cDNA Fragment by Degenerative Primers

Identification and characterization of the mouse cDNA was the prerequisite to generate a mouse with null mutation in MN/CA IX protein. To avoid the construction of a cDNA library from mouse stomach an attempt was made to clone *MN/CA9* cDNA fragment using an RT-PCR approach. The primers were designed according to the known sequence of human *MN/CA9* cDNA (Pastorek *et al.*, 1994). As a source of the RNA, a stomach of the wild type adult C57 BL/6J mouse was used. Ten *sense* and ten *antisense* primers from the whole coding region of the human *MN/CA9* cDNA were employed in all possible permutations. At least one *sense* and one *antisense* primer was designed for each protein domain of human *MN/CA9* cDNA. Out of all RT-PCR amplifications, only two fragments designated KAS2 (~560bp) and KAS3 (~350bp) were obtained. Both of them gave positive signals by Southern blotting with the human cDNA as a probe. Both fragments were cloned and the sequence analysis revealed 75% of nucleotide homology between the carbonic anhydrase domain coding sequence of human *MN/CA9* cDNA and both isolated fragments. The larger fragment KAS2 was used in further analysis (Fig.6).

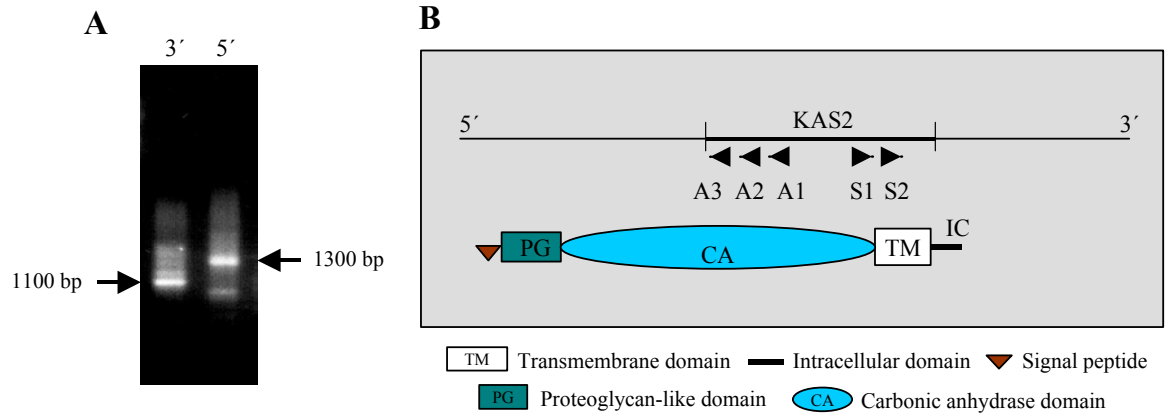

Fig. 6. Isolation of the full length of the murine *MN/CA9* cDNA by 3′and 5′ RACE (lane 3′and 5′, respectively). **(A)** 2µg of total RNA from wild type mouse was used for preparation of a specific cDNA product for 3′ and 5′ RACE. In 3′ RACE one round of semi-nested PCR was employed and in 5′ RACE two rounds of semi-nested PCR were employed. The specific products from 3′and 5′ RACE (1100 bp and 1300 bp, respectively) were analysed on 1% agarose gel. **(B)** Scheme of the murine *MN/CA9* cDNA with marked KAS2 fragment obtained from the RT-PCR using degenerative primers designed from the human *MN/CA9* cDNA. For the 3′and 5′RACE gene specific primers for the mouse *MN/CA9* cDNA (A1, A2, A3, S1 and S2) from the KAS2 fragment were designed.

5.1.2. Cloning of Murine MN/CA9 cDNA

To isolate the full-length of the novel murine cDNA we used the strategy of rapid amplification of cDNA ends (RACE). RACE was undertaken in 5' and 3' directions using the wild type adult mouse stomach mRNA. The 5´RACE was performed in two rounds of semi-nested PCR using gene-specific primers derived from KAS2 fragment. The PCR resulted in amplification of the 5'open reading frame (ORF) including initiation translation

A

```
   1  GCACGTACAG CCCGTCCACA GTGTGTCCTG GGACACCCCA GTCAGCTGCA TGGCCTCCCT
   1                                                          M  A  S
  61  GGGCCCCAGC CCCTGGGCCC CTTTGTCGAC CCCAGCCCCT ACTGCACAGC TGCTGCTGTT
   4  L  G  P  S    P  W  A    P  L  S    T  P  A  P    T  A  Q    L  L  L
 121  CCTGCTGCTC CAAGTGTCTG CTCAGCCCCA GGGCCTGTCC GGGATGCAGG GGGAGCCCTC
  24  F  L  L  L    Q  V  S    A  Q  P    Q  G  L  S    G  M  Q    G  E  P
 181  CTTGGGAGAC AGTTCATCTG GGGAGGATGA GCTGGGCGTG GATGTTCTGC CCAGTGAAGA
  44  S  L  G  D    S  S  S    G  E  D    E  L  G  V    D  V  L    P  S  E
 241  GGATGCACCT GAAGAGGCGG ATCCACCCGA TGGGGAGGAT CCACCTGAAG TTAATTCTGA
  64  E  D  A  P    E  E  A    D  P  P    D  G  E  D    P  P  E    V  N  S
 301  AGACAGGATG GAGGAGTCCC TTGGGTTAGA GGATCTATCG ACTCCCGAGG CTCCTGAGCA
  84  E  D  R  M    E  E  S    L  G  L    E  D  L  S    T  P  E    A  P  E
 361  CAGTCAAGGT TCCCACGGGG ATGAAAAAGG GGGTGGCCAC AGTCATTGGA GCTATGGAGG
 104  H  S  Q  G    S  H  G    D  E  K    G  G  G  H    S  H  W    S  Y  G
 421  CACCCTACTC TGGCCCCAGG TGTCCCCAGC CTGTGCTGGC CGCTTTCAGT CCCCGGTAGA
 124  G  T  L  L    W  P  Q    V  S  P    A  C  A  G    R  F  Q    S  P  V
 481  CATCCGCCTG GAGCGCACCG CATTCTGCCG CACTCTGCAA CCCCTGGAAC TTCTGGGTTA
 144  D  I  R  L    E  R  T    A  F  C    R  T  L  Q    P  L  E    L  L  G
 541  TGAGCTCCAG CCTCTCCCGG AACTGAGCCT ATCCAACAAT GGCCACACGG TACAGCTGAC
 164  Y  E  L  Q    P  L  P    E  L  S    L  S  N  N    G  H  T    V  Q  L
 601  TCTGCCGCCG GGGCTGAAGA TGGCTCTGGG ACCTGGGCAG GAATACCGGG CCTTGCAGTT
 184  T  L  P  P    G  L  K    M  A  L    G  P  G  Q    E  Y  R    A  L  Q
 661  GCATCTACAC TGGGGAACTT CAGATCACCC AGGCTCAGAA CACACAGTCA ATGGTCACCG
 204  L  H  L  H    W  G  T    S  D  H    P  G  S  E    H  T  V    N  G  H
 721  TTTCCCTGCT GAGATCCACG TGGTGCACCT CAGTACTGCT TTCTCCGAAC TTCATGAAGC
 224  R  F  P  A    E  I  H    V  V  H    L  S  T  A    F  S  E    L  H  E
 781  CTTGGGCCGC CCAGGAGGCC TGGCAGTTTT GGCTGCCTTT CTGCAGGAGA GCCCAGAAGA
 244  A  L  G  R    P  G  G    L  A  V    L  A  A  F    L  Q  E    S  P  E
 841  AAACAGTGCT TACGAACAGT TGCTGTCCCA TTTGGAAGAA ATCTCGGAGG AAGGCTCCAA
 264  E  N  S  A    Y  E  Q    L  L  S    H  L  E  E    I  S  E    E  G  S
 901  GATTGAGATC CCAGGTTTGG ATGTATCTGC ACTGTTGCCC TCGGACCTCA GCGCTACTA
 284  K  I  E  I    P  G  L    D  V  S    A  L  L  P    S  D  L    S  R  Y
 961  CCGATATGAA GGGTCTCTGA CCACACCTCC CTGCAGCCAG GGGGTCATCT GGACTGTGTT
 304  Y  R  Y  E    G  S  L    T  T  P    P  C  S  Q    G  V  I    W  T  V
1021  CAATGAGACA GTGAAACTGA GCGCTAAGCA GCTCCATACT CTCTCCGTTT CCTTGTGGGG
 324  F  N  E  T    V  K  L    S  A  K    Q  L  H  T    L  S  V    S  L  W
1081  ACCTCGTGAT TCTCGGCTAC AACTGAACTT CCGAGCCACG CAACCCTTGA ATGGGCGAAC
 344  G  P  R  D    S  R  L    Q  L  N    F  R  A  T    Q  P  L    N  G  R
1141  GATTGAGGCT TCCTTCCCTG CTGCAGAGGA TAGCAGCCCT GAGCCAGTCC ATGTGAATTC
 364  T  I  E  A    S  F  P    A  A  E    D  S  S  P    E  P  V    H  V  N
1201  CTGCTTCACT GCTGGTGACA TCCTAGCCTT GGTGTTTGGC CTTCTCTTTG CTGTCACCAG
 384  S  C  F  T    A  G  D    I  L  A    L  V  F  G    L  L  F    A  V  T
1261  CATCGCCTTC CTCCTACAGC TGAGGAGGCA GCACAGGCAC AGAAGTGGGA CCAAAGATAG
 404  S  I  A  F    L  L  Q    L  R  R    Q  H  R  H    R  S  G    T  K  D
1321  AGTTAGCTAC AGTCCGGCAG AGATGACAGA AACTGGAGCC TAATAAGGAG AAACCAGCTA
 424  R  V  S  Y    S  P  A    E  M  T    E  T  G  A    -  -
1381  AAGGAATCTG GAAACCTTGT CCTGTCCTGC CTGTTATACA GCCTCCTTTT TAACCACTAC
1441  GAAATCATTT CCATCTTTTT AACTTTCTTC TTTCCTTAAA GTACTGTGAT AGGAGCTAAC
1501  CGTGAAAAAA CAAGATTGGG CTCAATTCTT GCTGGGTTTT GATGGTTTTG AAGACAGGGT
1561  TTCTCTGTGT AGCCCTGGCT GTCCTGGGAC TCACTCTGTA GCCTAGGCTG GCCTTGAACT
1621  CAGAGATCCG ATTGCCTCTG CCTTCTTAGT GCCAGGACTG AGGGTATGTA CCACTACCAC
1681  CGCCACCCCG CAATTCTTGC TTTTATTCTG CAGTCAAATG CTCCACCACT GAGCTACACA
1741  CCCCTCCATC TTACTATGCA GGCAGACTGG CCTTGCATTG TGTATGTATG GTGATGGAGT
1801  TTGAAGCCAG GGTCTTACCT ACTAGGCAAG CGTTCTATCA CTGACCTAAG CCTCTCTAGT
1861  CCCTTCTCTT GAACCCTCTA TTCTCCTGTC CCAGCCTCTT GAATGCTGGG ATTACAGGAA
1921  TGCACCATCA TGCTTGGTCA TCCCAATTAT TTAAAAAAAA TATATAAATC TTCCTAGTAA
1981  AA
```

B

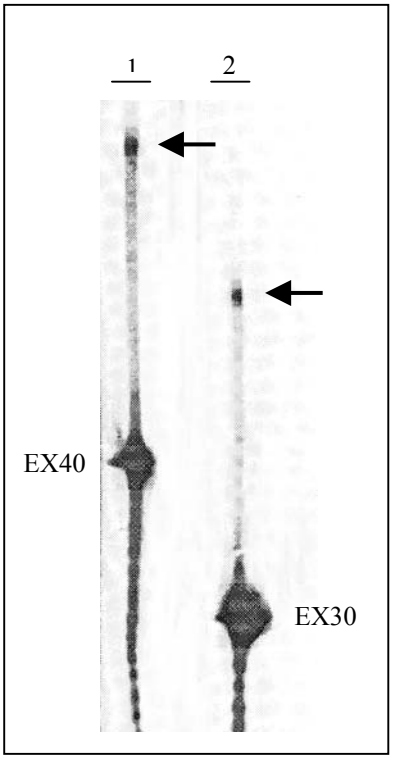

Fig. 7. (A) Nucleotide sequence of the *MN/CA9* cDNA. The deduced amino acid sequence is beneath the nucleotide sequence and is written in italic. The two plausible, modified polyadenylation signals are underlined. **(B)** Determination of the transcription initiation site of the *MN/CA9* gene by primer extension with *MN/CA9* cDNA specific primers EX30 (30bp) and EX40 (40bp). The arrows point to the transcription start site resulting from the primers EX40 (lane 1) and EX30 (lane 2).

codon ATG and a part of the 5' untranslated region (UTR). 3' RACE was carried out to define the 3' ORF and 3'UTR of the cDNA. For the 3'RACE also a gene-specific primer from KAS2 fragment was used. Both 5' and 3' RACE products were subcloned. The size of the 3'- end fragment obtained was approximately 1100bp and the 5'-end fragment had a length of approximately 1300bp (Fig. 6). The final ORF obtained by the RACE analysis consisted of 1311bp and had a coding capacity for a protein of 437 amino acid residues with a theoretical molecular mass of 47,3kDa. The cDNA contained 622 nucleotides of 3'-UTR (excluding the polyadenylated tail). No typical polyadenylation signal (AATAAA) was found in the 3'-UTR downstream of a double termination codon (TAA; TAA) and upstream of the poly(A) tail. Instead, two plausible modified polyadenylation signals could be used, e.g. AATATA and TATAAA found at positions 1958 and 1962, that is 18 bases and 14 bases, respectively, upstream of the poly(A) tail.

5.1.3. Mapping the Transcription Initiation

The 5'RACE method was not sufficient for identification of the transcription initiation site. It allowed us to recognize only the 32bp of 5'-UTR. This is due to the preferential amplification of the shorter fragments during the second round of the nested PCR. Thus, for the purpose of mapping the transcription initiation site we used the method of primer extension. Two reverse primers EXT30 (30bp) and EXT40 (40bp) from the known 5'-end extremity were used in separate reactions. Both primers showed a single product band (Fig. 7B). The size of the extended product was inferred from the truncated product ladder. The final 5′ end of the 5'UTR was 49bp upstream of the first ATG. The total size of the mouse *MN/CA9* cDNA was determined to be 1982bp (Fig. 7A).
These sequence data have been submitted to the EMBL database (Ortova Gut *et al.*)

5.1.4. Single Splicing Variant of Murine MN/CA9 cDNA

RNA from the wild type mouse stomach was analyzed by Northern blot hybridization. The full-length murine *MN/CA9* cDNA was used as a probe. The analysis did not reveal any splicing events. A single product of a size around 2kb was found. Based on the result of this analysis together with the result of primer extension experiment we can clearly conclude that MN/CA IX is translated from a single splicing variant mRNA.

5.1.5. Determination of the Primary Structure of the Murine MN/CA9 cDNA

For the sequence analysis, oligonucleotide primers (24-mers) designed to provide sequencing sites at 200 to 300 intervals along the cDNA were used. The untranslated regions were sequenced two or three times in overlapping segments whereas the expected translated portion was sequenced using three to four overlapping regions (Fig. 7A).

A sequence similarity search in databases indicated that the encoded protein is a member of the α-carbonic anhydrase gene superfamily. An initial BLAST sequence similarity search of the public expressed sequence tag (dbEST) nucleotide databases (Altschul *et al.*, 1997) with the mouse cDNA sequence disclosed a total of two results. They both corresponded to the human orthologue *MN/CA9*. Under the Accession N° X66839 the cDNA sequence and the genomic sequence with corrections of the previous one under the N° Z54349 were found. Amino acid sequence comparison of these orthologues did not show a high level (69,5%) of sequence identity.

5.1.6. Expression Pattern of the Murine MN/CA9 mRNA

A quantitative analysis of *MN/CA9* mRNA was undertaken using a ribonuclease protection (RNP) assay (Tab. 2). A riboprobe of 170bp in size was designed to detect the 3' end of the carbonic anhydrase domain. The expression pattern confirmed the highest abundance of *MN/CA9* in the mouse stomach. Other tested organs exhibited lower or no expression. There was a significant difference in the expression pattern between mouse and human colon.

Stomach	+++
Intestine - proximal	++
Colon - distal	++
Liver	-
Spleen	-
Brain	+
Kidney	+
Embryonic stem cells	-
Embryo E12	-
Embryo E18	+

Tab. 2. Expression of murine *MN/CA9* mRNA as detected by ribonuclease protection assay. Expression levels denoted by +++ were considered as very strong; ++ strong; + weak and – no signal detected.

In human colon, the MN/CA IX protein is expressed in a gradient-like manner. However, in the mouse the signal intensity was at the same level in the proximal and in the distal part of

the colon. This distribution is similar to the expression pattern in the rat intestine (Pastorekova et al., 1997). Noteworthy, the RNP signal was also present in a sample of mouse embryo at the age of embryonic day E18 indicating that MN/CA IX protein may be involved in formation of the gastrointestinal tract.

5.1.7. Expression of Murine MN/CA9 cDNA in Tumor Cell Lines and Tumor Tissue Sample

Previous investigations showed MN/CA IX protein expression in several types of human clinical specimens and cell cultures (Zavada *et al.*, 1993). To assess whether also the mouse *MN/CA9* mRNA is expressed in neoplastic samples, its expression in murine cell lines and spontaneous mammary tumor tissue sample was investigated. Using the highly sensitive RT-PCR method it was possible to detect the presence of *MN/CA9* cDNA in three mammary tumor cell lines (TS/A; GR/3; MM5). The control cell line representing the normal mammary gland (NMG) as well as other tumor cell lines, RENCA (renal carcinoma cell line) and J558 (B lymphoma cell line), were found to be *MN/CA9* negative (Fig. 8).

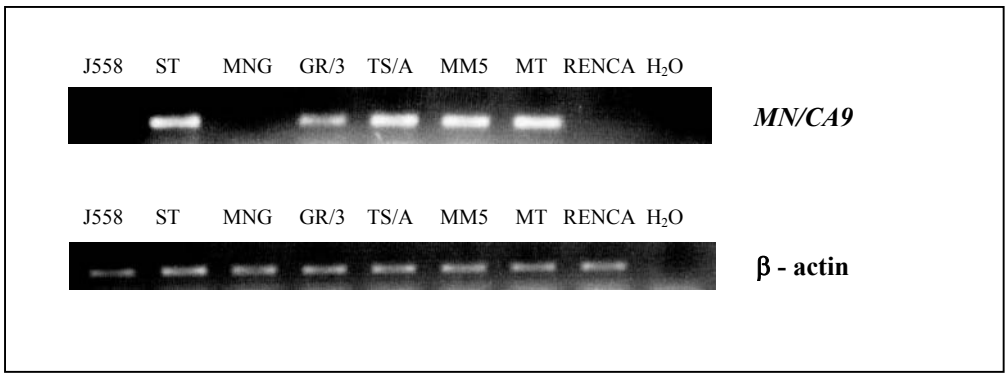

Fig. 8. Expression pattern of *MN/CA9* mRNA in mammary tumor carcinoma cell lines - TS/A, GR/3, MM5; B-lymphoma cell line - J558; renal cell carcinoma cell line - RENCA; normal mammary gland cell line - NMG; mouse mammary gland tumor tissue sample - MT and mouse stomach sample - ST. 1μg of total RNA was used for reverse transcription and 3μl of the cDNA was subjected to PCR to determine the expression. To control the quality of the RNA, the efficiency of reverse transcription and the PCR amplification, β-actin was used.

During our investigation we were able to record one case of spontaneous mammary tumor in a BALB/c female mouse in our animal facility. The origin of the tumor was confirmed by histological examination. This rare malignant tissue sample was examined by RT-PCR for presence of *MN/CA9* cDNA and was found to be positive (Fig. 8). These results strongly support the idea that the mouse MN/CA IX may be also implicated in oncogenesis.

5.1.8. Comparison of Murine cDNA to Human MN/CA9 cDNA

The carbonic anhydrases are subdivided into several groups on the basis of structural characteristics of their domains and their subcellular localization. Murine MN/CA IX protein has a predicted N-terminal extracellular region (aa 48-389), a transmembrane region (aa 390-411), and an intracellular C-terminus (aa 412-437). The presence of a potential signal peptide (aa 1-31) cleavage site, between position aa 31 and 32, indicates that murine MN/CA IX protein is directed across the cytoplasmic membrane. The extracellular part is composed of two distinct domains - a proteoglycan-like domain (aa 48-107) and carbonic anhydrase domain (aa 112-369). It is presently unknown whether the glycosaminoglycan attachment sites in the proteoglycan-like domain are utilized or not. The transmembrane domain (aa 390-411) and a short cytoplasmic domain (aa 412-437) constitute the intracellular part. A similar domain composition was described for human cDNA (Pastorek *et al.*, 1994; Opavsky *et al.*, 1996).

Mouse and human proteins have 69,5% sequence homology on the predicted amino acid level. Most of the sequence differences between mouse and human are in the N-terminal proteoglycan-like domain. Although the total size of the mouse cDNA is longer (1982bp versus 1552bp), the mouse coding region is shorter by 66bp. This is due to several gaps. The first significant gap of 4 amino acids lies in the signal peptide (aa 17-18). Another important gap of 12 amino acids is situated in the proteoglycan-like domain (aa 79-80). The other gaps are probably less important since their location is in between the structural domains.

In the catalytically active CA isozymes, key amino acids of the active site include His94, His96, Glu106, His119 and Thr199 (employing the mature human CA I nomenclature in which position 1 is the first residue after the N-terminal Met, see Hewett-Emmett and Tashian, 1996). Three histidine residues creating the enzyme core tetrahedrally co-ordinate a zinc ion via their imidazoles (in conjunction with a water molecule that provides the hydroxide ion). Additionally, Glu106 and Thr199 contribute to the hydrogen bonding network with the zinc OH^-, restricting its orientation and so maintaining the catalytically competent structure (Christianson and Cox, 1999). Of these five residues, one substitution was found in the mouse MN/CA IX (Thr199→Ser). In the human cDNA all five residues are conserved. The core of the two homologues is highly conserved (mouse - SEHTVNGHRFPAEIHVV and human - SEHTVEGHRFPAEIHVV).

Both human and mouse MN/CA IX proteins have the highest conservation in the

transmembrane anchor and in their carbonic anhydrase domain. Both homologues have a consensus sequence for a potential N-glycosylation site in the same position within the carbonic anhydrase domain (mouse aa 325 and human aa 346). Although the intracytoplasmic region does not share very high homology, it seems that on a functional level the homologues resemble each other. In the intracytoplasmic region both proteins have a myristilation consensus sequence at the same position (mouse aa 420 and human aa 442) and Ser phosphorylation sites close to each other (mouse aa 428 and human aa 448).

5.1.9. Purification of the Mouse MN/CA IX *Protein*

The mouse MN/CA IX was purified by affinity chromatography using a gel containing p-aminomethylbenzenesulfonamide coupled to agarose beads. This procedure was previously used for other active carbonic anhydrases (Falkbring *et al.*, 1972). Human MN/CA IX is a very high activity isozyme (Karhumaa *et al*., 2000) and its purification was successful by this method modified by Zavada *et al.*, 2000.

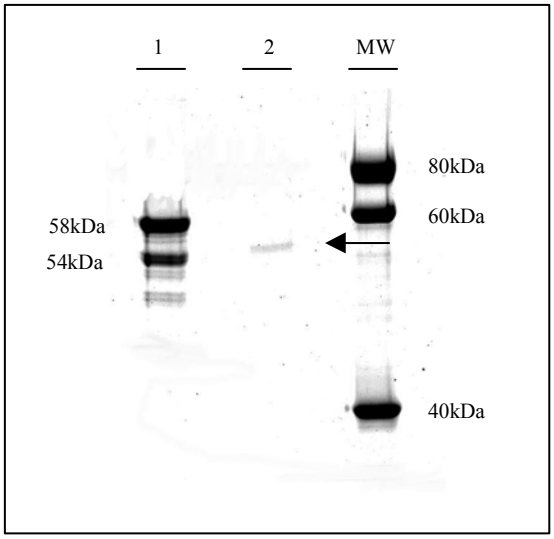

Fig. 9. Affinity chromatography purified murine MN/CA IX protein (lane 2) separated on 8% acrylamide gel stained with Coomassie Blue. In the lane - 1 - is purified human MN/CA IX protein (generous gift from Dr. Zavada). Lane - MW are the molecular weights in kDa. The arrow is pointing at the single protein band of purified murine MN/CA IX (lane 2).

The TS/A cell line was used as a source of mouse MN/CA IX protein, since it was found to overexpress *MN/CA9* mRNA. The protein extract was prepared with Triton X-100 and applied in a single cycle of adsorption. Acetazolamide is a potent carbonic anhydrase inhibitor and acts competitively with the sulfonamide groups covalently fixed to the adsorbent. The enzyme was eluted in aliquots from the column as an enzyme-complex. The

high purity protein aliquots that contained highest amounts of MN/CA IX were joined. The enzyme purity was confirmed on acrylamide gel stained with Coomassie Blue. A single prominent band at the size of 54kDa was detected (Fig. 9).

The band was cut out of the gel and characterized by MALDI-MS (Matrix-Assisted Laser Desorption/Ionisation Mass Spectrometry). The predicted mass of MN/CA IX corresponded by 99,5% to tryptic fragments identified by MALDI-MS.

5.1.10. Preparation of Antibody Specific to Mouse MN/CA IX *Protein*

The mouse monoclonal antibody M75 raised against human MN/CA IX protein recognizes the N-terminal proteoglycan domain (Pastorekova et al., 1992). The expression of MN/CA IX was studied in several vertebrates. The M75 antibody crossreacted in Western blot analysis with MN/CA IX proteins isolated from the stomach of rat, guinea pig and chick (Pastorekova et al., 1997). In our preliminary it was not possible to detect any protein in the mouse stomach tissue samples by using MAb M75.

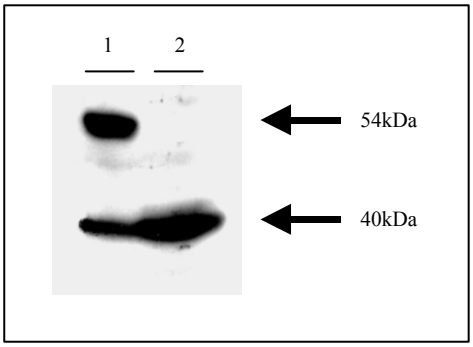

Fig. 10. Western blot analysis of the mouse MN/CA IX protein. Crude cell lysates was isolated from the transfected NIH 3T3 by *MN/CA9* cDNA (lane 1) and from the non-transfected NIH 3T3 (lane2) cell line. 10µg of the total protein extract was used for each lane and analyzed on 10% polyacrylamide gel. MN/CA IX was detected by polyclonal serum antibody anti-PG-MN. The upper arrow points to the MN/CA IX, a band of the size 54kDa. At the size 40kDa is shown an unspecific band, as a control of the quality of used protein.

The absence of functional anti-mouse MN/CA IX antibody prompted us to prepare a polyclonal anti-mouse antibody against synthetic peptides. Two oligopeptides were selected using computer prediction of the antigenic determinants from the mouse MN/CA IX protein. One represented a part of the proteoglycan-like domain (CPPDGEDPPEVNSE) and the second peptide was a part of the carbonic anhydrase domain (GTSDHPGSEHTVNGC). Both oligopeptides were synthesized with the C-terminal Cys, through which the peptides were coupled with KLH and each was used for immunization of two rabbits in a 77 days protocol (Sigma Genomics). Neither of the rabbits produced satisfactory levels of antibodies

directed against the CA domain oligopeptide. In the case of the oligopeptide derived from the PG-like domain both rabbits produced serum-antibody of relatively good quality (anti-PG-MN). The specificity of the anti-PG-MN antibody against the oligopeptide (data not shown) and the purified MN/CA IX protein was tested (Fig. 10). The serum-antibody anti-PG-MN was used for Western blotting analysis and for immunohistochemical staining.

5.2. ISOLATION AND CHARATERIZATION OF MN/CA9 GENE

5.2.1. Isolation and Characterization of Murine MN/CA9 Genomic Clones

In order to determine the organization of murine *MN/CA9* gene, genomic clones were isolated. A mouse embryonic stem (ES) cell 129/Ola genomic library (Genome Systems) was screened with the full size *MN/CA9* cDNA. These screens yielded three genomic clones in a pBAC108L (Bacterial Artificial Chromosome108L). pBAC108L clones contained inserts of approximately 200kb. Restriction maps of these three clones that hybridized to 5' and 3' fragments of murine *MN/CA9* cDNA were prepared.

Restriction mapping and Southern blot analysis revealed that only one pBAC108L clone (BACM-355(G13)) contained the full size genomic sequence and therefore was analyzed in depth. The authenticity of the clone was confirmed by restriction digestion and Southern blot analysis of a mouse wild type genomic DNA. Three overlapping genomic fragments of the murine *MN/CA9* gene were subcloned into a pBluescript from the BACM-355(G13) clone. The longest KpnI fragment encompassed ~10,5kb and contained the promoter sequence and exons 1 to 5. The shortest fragment (~1400bp), also derived from KpnI restriction digestion, was identified to code for exons 7 to 11. The EcoRI genomic fragment (~6,5kb) contained exons 1 to 9 and 1300bp of a promoter. This EcoRI fragment was later used for construction of the targeting vector.

5.2.2. Organization of Exons and Introns in Mouse MN/CA9 Gene

The whole mouse *MN/CA9* gene was sequenced. Its structure was analyzed by comparison of the sequence information from the murine *MN/CA9* cDNA and the known human genomic sequence (accession N° Z54349). The resulting genomic situation was very similar to the human one. *MN/CA9* gene is composed of 11 exons and 10 introns and covers 6,7kb of the mouse genome. Table 3 shows the size of each exon and intron, the junction

sequences, and the location and phasing of each intron in the *MN/CA9* gene. The whole coding sequence is spread in small exons. The exons vary in size from as few as 27bp (exon 9) to 171bp (exon 3), excluding 5' and 3' terminal exons, which are 389 and 686 nucleotides in length, respectively. The average internal exon size is 100bp, close to the average vertebrate internal exon size of 137bp. The introns vary in size from 82bp (intron 4) to 1562 (intron 6). The splice donor and acceptor sites of all ten introns conform to the consensus sequence GT-AG (Mount, 1982). Of the introns in the *MN/CA9* gene, 3 are type 0, where introns occur between codons (i.e., introns 4, 5 and 7), 6 are type 1, where introns interrupt the first and second base of the codon (i.e., introns 1, 2, 3, 6, 8 and 9), and only one intron is type 2, interrupting the second and third base of the codon (intron 10). The mouse intron junction types are identical to the human genomic situation. Overall, approximately 29,5% (1,9 / 6,7kb) of the gene corresponds to exon sequence.

Exon 1 encodes the 5' untranslated region, the signal peptide and the proteoglycan-like domain. The central, carbonic anhydrase domain is encoded by the exons 2-8. Exon 10 represents the transmembrane anchor. Finally, exon 11 encompasses the C-terminal cytoplasmatic tail and the 3' untranslated region.

				Sequence at exon-intron junction			AA at junction			
Exon	Exon size (bp)	Intron	Intron size (bp)	5' splice	donor	3'splice	acceptor	AA	Position	Type
I	389	1	924	AAAAAG	**gt**aagt	atgc**ag**	GGGGTG	G	114	1
II	30	2	261	ATGGAG	**gt**aaga	tccc**ag**	GCACCC	G	124	1
III	171	3	119	ACACGG	**gt**gagg	acgc**ag**	TACAGC	V	181	1
IV	143	4	82	GCTGAG	**gt**gggg	ctct**ag**	ATCCAC	E/I	228	0
V	93	5	987	CTGCAG	**gt**accc	ctgc**ag**	GAGAGC	Q/E	259	0
VI	67	6	1562	GAGGAA	**gt**tggt	ccgt**ag**	GCTCCA	G	281	1
VII	158	7	157	AAGCAG	**gt**taga	cccc**ag**	CTCCAT	Q/L	334	0
VIII	136	8	134	AGCCAG	**gt**gccc	cttc**ag**	TCCATG	V	380	1
IX	27	9	413	CTGCTG	**gt**gagt	ttcc**ag**	GTGACA	G	389	1
X	82	10	111	GCACAG	**gt**atct	ctat**ag**	GCACAG	R	416	2
XI	686	end		GTAAAA						

Tab. 3. Intron-exon junctions in murine *MN/CA9* gene. Nucleotide sequences indicated at the intron (lowercase letters) and exon (uppercase letters) junctions. Exons are numbered from the 5' end as illustrated in Fig. 11. The size of introns and exons are indicated in basepairs (bp). The amino acid (AA) interrupted by an intron is indicated by a single letter and its position is shown. For type 0 introns, the 2 amino acids on each side of the intron are given.

5.2.3. MN/CA9 is a Single Copy Gene

Important information in a gene targeting strategy is the gene copy number in the haploid mouse genome. Genomic Southern blot analysis was performed using mouse ES cell genomic DNA digested with restriction endonucleases XbaI, EcoRI, and KpnI. The Southern blot was probed with mouse *MN/CA9* cDNA representing the first 4 exons of the

mouse gene. The hybridization pattern indicated a single copy gene per haploid mouse genome (data not shown).

5.3.CONSTRUCTION OF MN/CA9 DEFICIENT MOUSE

5.3.1. Targeting Strategy for Inactivation of MN/CA9 Gene by Homologous Recombination

In order to investigate the potential role of *MN/CA9* gene in gastrointestinal tract development and in carcinogenesis, a mouse lacking a functional product of this gene was generated by homologous recombination.

Once the *MN/CA9* gene had been cloned and characterized, a strategy designed to obtain a mouse with a null mutation in *MN/CA9* gene locus was followed.

The genomic fragment EcoRI-HindIII (5,9kb) of *MN/CA9* gene was used for the targeted mutagenesis. It contained 1,3kb of the promoter, exons 1-6 and introns 1-6. These exons in the MN/CA IX protein represent the signal peptide and proteoglycan like domain (exon 1) and part of the carbonic anhydrase domain (exon 2-9). A replacement type of vector (p*MN/CA9*-neo) was used to introduce a specific mutation into the mouse *MN/CA9* gene. To inactivate the *MN/CA9* gene, 14bp of the proteoglycan-like domain located in the first exon were replaced by a cassette formed by the phosphoglycerate kinase (PGK) and aminoglycoside phosphotransferase (neo) resistance gene. The PGK-neo cassette was cloned in the opposite transcriptional orientation. This cassette was also used as a positive selection marker. The p*MN/CA9*-neo construct contained 1,4kb the 5'-homology and 4,5kb with the 3'-homology to *MN/CA9* genomic sequence (Fig. 11).

Homologous recombination of the p*MN/CA9*-neo vector with the endogenous locus was used to ensure inactivation of the *MN/CA9* gene by shift of the reading frame. At the same time the insertion of the PGK-neo gene introduced multiple stop codons in all reading frames. Furthermore, reverse orientation of the neomycin phosphotransferase gene with a strong promoter supported destabilization of any secondary transcript.

The targeted disruption of the *MN/CA9* gene was monitored with the 3'-probe on the genomic level by the change in size of the EcoRI fragment (6,5kb). On the genomic level the external 3'-probe was a HindIII-EcoRI fragment (688bp) externally flanking 3' homology region of the targeting vector. Insertion of the PGK-neo cassette (1,8kb) increased the size of EcoRI fragment from 6,5 to 8,3kb (Fig. 11). To eliminate the possibility of simple insertion of the target vector, the external 5'-probe (XbaI-EcoRI; 668bp) was also

designed. By insertion of the PGK-neo cassette a new XbaI restriction site was introduced and the 5'-probe monitored the decrease of size of the XbaI fragment from 4kb to 2kb.

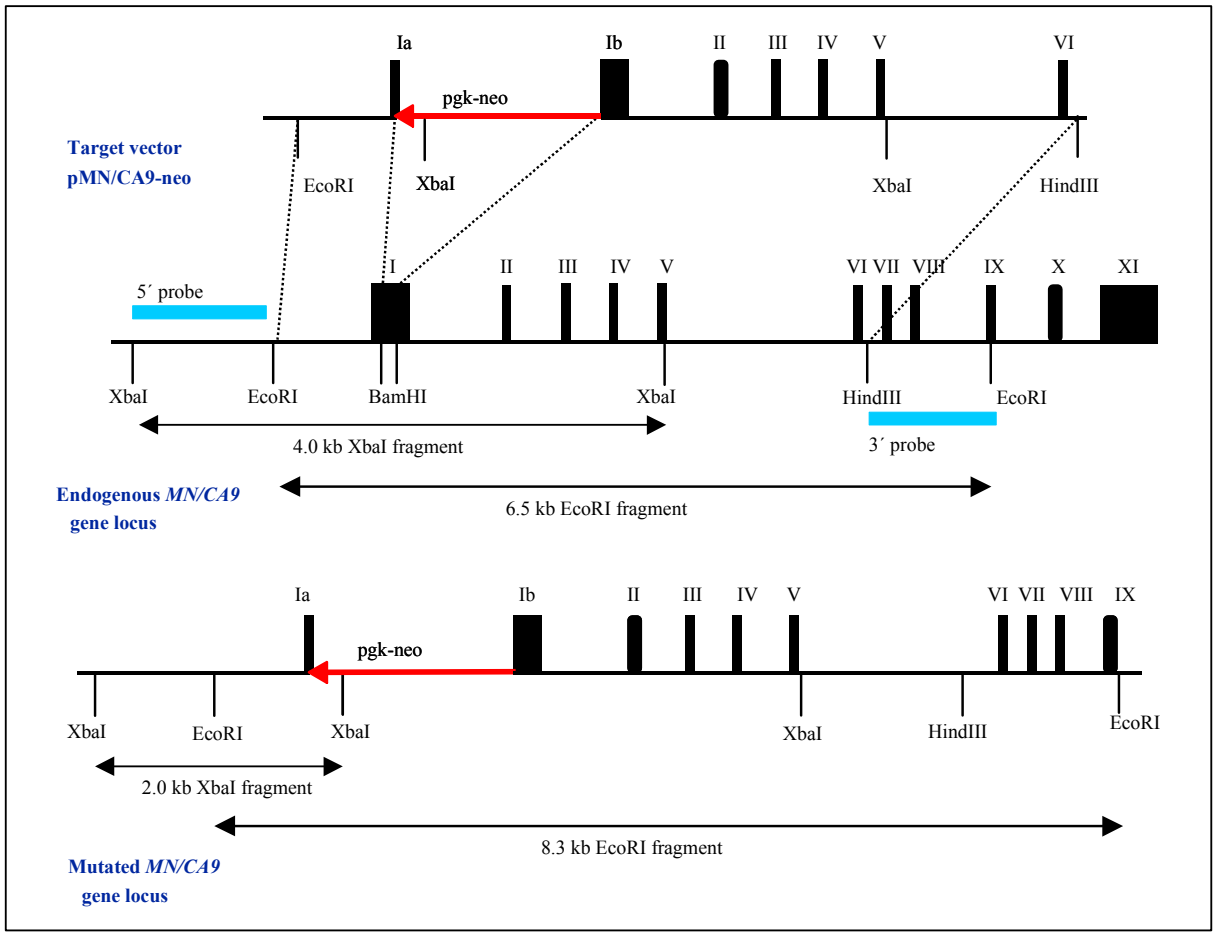

Fig. 11. Targeted disruption of the murine *MN/CA9* gene. Schematic representation of 9kb of the targeting construct, normal murine *MN/CA9* gene is shown in the middle, and resulting disrupted locus. The numbered closed boxes (I-XI) denote the eleven translated exons of the gene. The double-headed arrow indicates the endogenous 6,5kb and 4,0kb (EcoRI and XbaI) fragments characteristic of the wild-type gene as defined using a labeled DNA probes derived from the 3´or 5´ end not included in the targeting vector. The replacement target vector was constructed to inactivate the *MN/CA9* gene. The first exon was interrupted by deletion of 14bp and insertion of a neomycin resistance cassette. After homologous recombination of the construct the endogenous locus of the *MN/CA9* gene is inactivated by shift of the reading frame and at the same time the insertion of the neo gene introduces multiple stop-codons in all reading frames. The reverse orientation of the neomycin gene - as indicated by the bold arrows, with a strong promoter supports destabilisation of any secondary transcript.

5.3.2. Cloning of the Targeting Vector pMN/CA9-neo

Genomic fragment EcoRI (6,5kb) of *MN/CA9* gene was used to construct the targeting vector. This fragment was isolated from a mouse ES 129/Ola genomic library (Genome Systems) using murine cDNA as a probe, as described in the chapter 5.2. The genomic library from the 129/Ola background was identical to the ES cell line used later for the targeted mutagenesis. The EcoRI fragment was subcloned into pBluescript II KS and

characterized by a restriction mapping and by sequencing. For cloning of the 3' and 5' gene regions, modified pBluescript II KS (pB-B) was used. In the pB-B plasmid the restriction site BamHI was deleted by PstI and XbaI restriction digestion. The pB-B plasmid was purified on a gel and religated back blunt. The *MN/CA9* genomic fragment EcoRI-HindIII (5,3kb) that originated from the EcoRI (6,5kb)-pBluescript genomic subclone, was cloned into pB-B plasmid. Using the BamHI restriction enzyme 14bps were deleted from the first exon. Between the blunted BamHI ends the blunted PGK-neo cassette was inserted in the 3'-5' orientation towards the transcriptional initiation site of the *MN/CA9* gene. Using this approach we obtained a 5' homology fragment (1,4kb) and a 3'-homology fragment (4,5kb) interrupted by a PGK-neo cassette. All cloning steps were controlled for the correct orientation of the cloned fragments by sequencing. The total size of the p*MN/CA9*-neo vector was 7,7kb, of it the homologous regions of the *MN/CA9* gene were 5,9kb. High purity targeting vector was linearized with EcoRI restriction enzyme and electroporated into ES-cells. Figure 11 shows the cloning schema of a p*MN/CA9*-neo vector.

5.3.3. Generation of ES-cell Clones with Mutated MN/CA9 Allele

A negative-selection strategy allowed us to recognize and to detect among the electroporated ES-cell clones those that carried the mutated DNA.

The E14 ES-cell line was transfected with the linearized p*MN/CA9*-neo target vector through electroporation. The electroporated clones were kept under conditions maintaining the pluripotency. The G418 selection (8-10 days) was initiated after 48 hours of undisturbed growth of the ES-cells with daily medium change. The G418 selection enriched those clones that underwent homologous or non-homologous recombination and carry the PGK-neo resistance cassette. Out of $1x10^6$ plated cells about 500-800 clones survived this procedure. Those colonies that still maintained a discrete border were individually picked under a microscope (400 - 600 clones) and expanded on the 96-well plate. After two days these clones were split 1:1, one half was frozen immediately on the replica plate. This early freezing of the clones allowed us to avoid a negative influence of useless passages, which could result in loss of capacity of the ES-cells to participate in the germline transmission (Fedorov *et al.*, 1997). The second half of the ES clones was used for DNA isolation. Additional expansion on 24-well plates ensured a sufficient amount of cells for the DNA isolation. After several days of cultivation the DNA was isolated directly in the 24-well plates (Laird *et al.*, 1991).

To test the homologous recombination, genomic DNA of each separate clone was digested with EcoRI restriction enzyme and separated on an agarose gel. Digested DNA was tested by Southern blot analysis with an EcoRI/ HindIII 3'-probe (Fig. 11). It was possible to

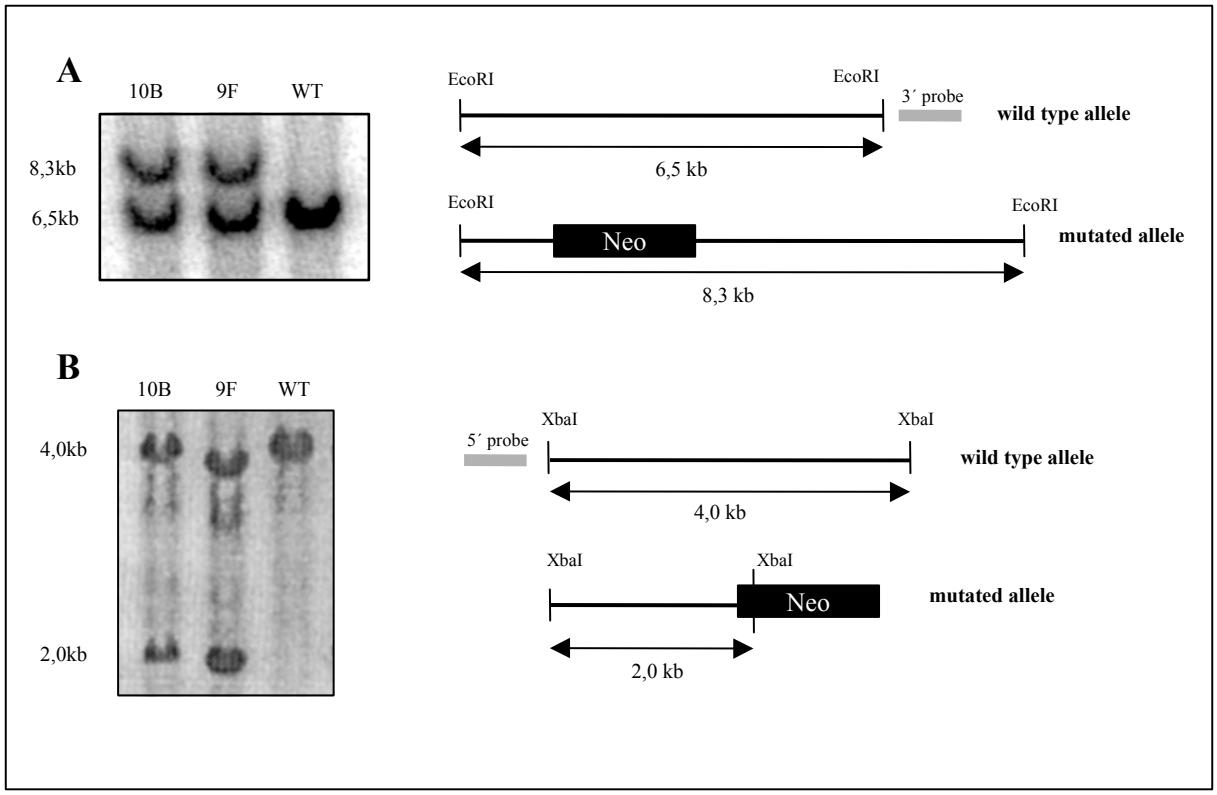

Fig. 12. Southern blot analysis of the ES-cell clones for the mutation in the *MN/CA9* gene locus after the electroporation of the targeting vector and negative selection using G418. 15µg of genomic ES-cell DNA from resistant clones and from control wild type ES clone were digested with EcoRI **(A)** or XbaI **(B)** and separated on 1% agarose gel. In Southern blot analysis the external, ^{32}P-labeled probes 3´and 5´ monitored the increase in the size **(A)** or decrease in the size **(B)** of the *MN/CA9* gene locus. The diagrams beside show a portion of the mouse *MN/CA9* gene locus with relevant restriction sites. The double-headed arrows indicate size of the wild type allele and increase (for EcoRI restriction digestion and monitored by 3´probe) or decrease (for XbaI restriction digestion and monitored by 5´probe) of the mutated allele.

detect 8 clones that carried the mutated allele with the expected increase in size from 6,5 to 8,3kb (Tab. 4; Fig. 12A). Two of these positive clones were chosen (10B and 9F), thawed from the frozen replica plate and brought back to culture. Before injection of the 10B and 9F clones into a foster mother both were analyzed by Southern blotting. Both clones were digested by EcoRI and hybridized with the EcoRI/ HindIII 3'-probe as well as by XbaI and the XbaI/EcoRI 5'-probe. This strategy excluded the possibility of simple insertion of the targeting vector (Fig. 12B).

N° of electroporation	Total N° of clones	N° of positive clones	Destiny of positive clones
1	500 clones	1 positive	died
2	200 clones	5 positive	10B and 9F injected, other clones frozen
3	700 clones	2 positive	clones frozen

Tab. 4. Frequency of positive clones in three different electroporations.

5.3.4. Frequency of the Homologous Recombination

The frequency of the homologous recombination (T = Targeting efficiency) is the number of homologous recombinations in proportion to non-homologous integrations in the genome:

$$T = \frac{\text{Number of clones positive for homologous recombination}}{\text{Total number of tested clones}} = \frac{8}{1400} = 1 : 175$$

It means that for the particular targeting vector p*MN/CA9*-neo, with 5,3kb of total homology to the endogenous gene locus, the detectable homologous integration occurred in one of 175 clones.

5.3.5. Generation of Chimeric Mice with ES-cell Clones 10B and 9F (MN/CA9$^{+/-}$)

Once ”targeted clones” 10B and 9F were identified, the next step involved the production of chimeric embryos. Both selected clones (for each 8-15 *MN/CA9*$^{+/-}$ ES cells) were injected into the inner cavity of a blastocyst (C57 BL/6J mouse strain). These chimeric blastocysts were transferred into uteri of foster mothers (BALB/c mouse strain) who brought them to term. Table 5 shows the efficiency of the embryo-transfer and the number of chimeric mice obtained. For clone 9F the transfer was successful in 20% and for clone 10B in 10% of the cases. Chimerism of the offspring was observed in 57% for clone 9F and 89% in the case of clone 10B. These results are in agreement with expected values for optimal experimental conditions.

Clone	9F	10B
Number of injections	2	3
Number of injected blastocysts	40	81
Total number of offspring	7	9
Final number of chimeric offspring	4	8

Tab. 5. Generation of chimeric mice with the ES-cell of the clones 9F and 10B

5.3.6. Chimeric Mice from Clones 10B and 9F are Germline Transmitters

One of the milestones during generation of transgenic mouse is if the ES cells enter the germline as demonstrated by breeding. The capacity of the chimeric mice to transmit the desired mutation to the offspring was tested by mating them with C57 BL/6J mice. Germline transmission was distinguished by the brown coat color of their offspring. The brown color resulted from their mixed background (129/Ola x C57 BL/6J). Among the brown animals, 50% should be heterozygotes that carry one ”wild type” allele and one mutated allele. The decision of whether or not to breed a particular chimera depended on the level of its coat chimerism (see Tab. 6).

Clone 10B *MN/CA9*$^{+/-}$			
Sex	Level of chimerism	Number of offspring	Brown offspring
male	70%	33	33
male	80%	58	47
male	75%	49	18 all $^{+/+}$
male	75%	41	6 all $^{+/+}$
male	90%	sterile*	-
male	under 30%	not bred	-
male	80%	not bred*	-
female	over 95%, red eyes	sterile	-
Clone 9F *MN/CA9*$^{+/-}$			
male	60%	sterile*	-
male	80%	58	47
female	40%	sterile	-
female	40%	sterile	-

Tab. 6. The Level of chimerism and the efficiency of chimeric mice to transmit mutation in *MN/CA9* gene. The asterisk * marks the animals with aberrant development of reproductive organs.

The disrupted *MN/CA9* gene was indeed transmitted through the germline in the cases of clones 10B and 9F (Tab. 6). In clone 10B out of 8 chimeras four were capable of germline transmission, one was not bred for its low chimerism and two were not bred but killed because they showed aberrances in development of their genitals. In clone 9F only one out of four animals was a germline transmitter. The other three animals were sterile.

The first (”F1”) generation of offspring from the chimeric founders (germline transmitters) also included heterozygous animals. Genotype of brown colored mice was determined by Southern blot analysis of their genomic DNA obtained from tail biopsies. EcoRI restriction digestion of genomic DNA was detected by a 3’-probe. Heterozygous animals were intercrossed to produce a second (”F2”) generation. The F2 generation included individuals homozygous for both wild type alleles (+/+), heterozygotes (+/-) and homozygotes with both alleles mutated (-/-).

5.3.7. Mendelian Transmission of the Mutation to the ”F2” Generation

Genotypic analysis of 286 3-week-old offsprings of *MN/CA9* heterozygous mice intercrosses demonstrated that homozygous mutants were born at the expected Mendelian ratio (25%). The ratio of the genotypes of mice resulting from clone 10B were 54 +/+; 118 +/-; 54 -/-, and for clone F9 15 +/+; 33 +/- and 12 -/- with an even distribution of both sexes

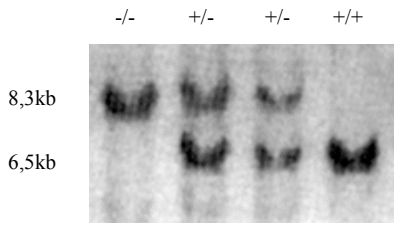

Fig. 13. Southern blot analysis after intercrossing of heterozygous *MN/CA9*$^{+/-}$ mice. The genomic DNA was isolated from the tails of 3 weeks old mice, 10µg of the genomic DNA were digested with EcoRI and hybridized with the ^{32}P-labeled 3´probe, as described in figure 12. Bands are indicated corresponding to wild type (6,5kb) and mutated (8,3kb) genes.

in these clones. From this result we can conclude that targeted mutation in the MN/CA9 gene does not have any influence on embryonal lethality. The results obtained from Southern blot analysis of tail genomic DNA from animals representing the three different genotypes are presented in Figure 13.

5.3.8. Mice with Mutation in MN/CA9 Gene Express Truncated MN/CA9 mRNA

To determine whether the gene targeting resulted in a null-mutation, transcript of the *MN/CA9*$^{-/-}$ gene was analyzed. Northern blot analysis of total RNA from stomachs of *MN/CA9*$^{-/-}$ and *MN/CA9*$^{+/+}$ mice showed a single *MN/CA9* mRNA species for *MN/CA9*$^{-/-}$ mice of similar size and same intensity as for *MN/CA9*$^{+/+}$ mice (Fig. 14).

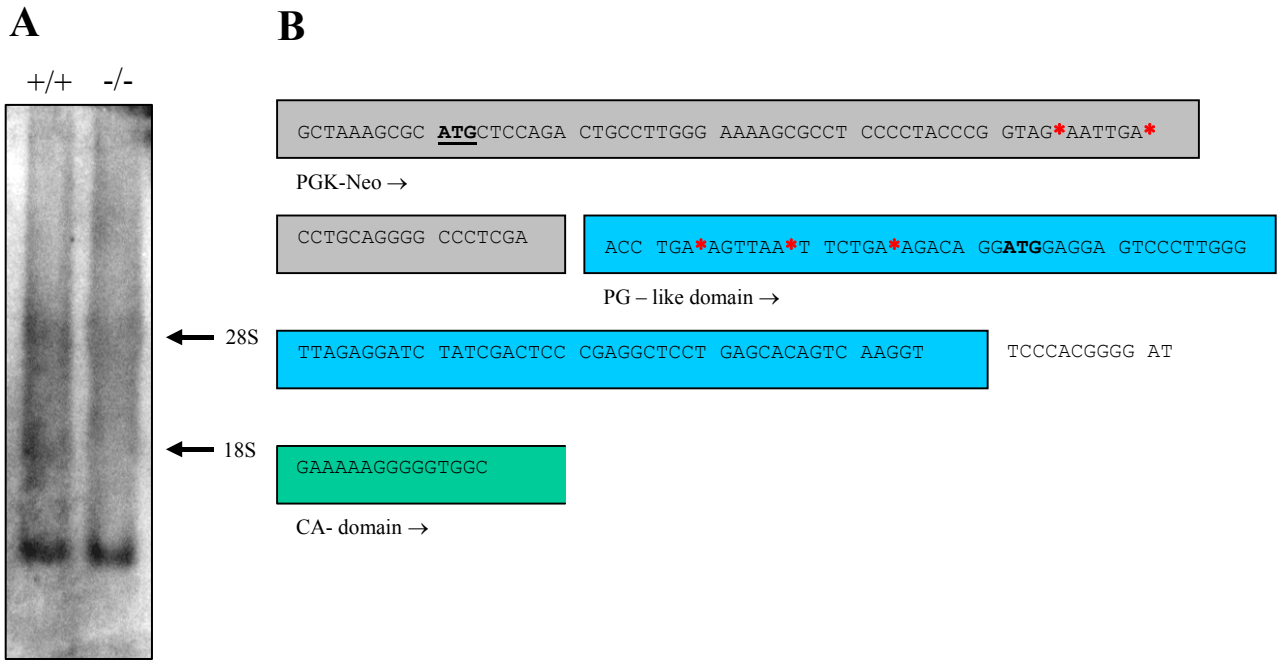

Fig. 14. RNA analysis of *MN/CA9* RNA. **(A)** Northern blot analysis of the genotype-specific expression pattern. Total RNA was isolated from representative *MN/CA9*$^{-/-}$ (lane -/-) and normal (+/+) mice. 20µg of RNA sample was separated on a denaturing agarose RNA-gel and hybridized with ^{32}P-labelled murine *MN/CA9* specific probe representing the full length of the cDNA. Quantitative normalization was confirmed using a probe for the β-actin (data not shown). Size was estimated from 18S (2300 nucleotides) and 28S (6300 nucleotides) rRNAs.
(B) 5'end analysis of the mutated mRNA isolated from *MN/CA9*$^{-/-}$ mice by 5´RACE. As a result of post-transcriptional modifications the majority of the PGK-neo cassette was spliced out together with the initiation codon ATG from the signal peptide (not shown). The remaining sequence of the PGK-neo cassette (gray filled bars) as identified by sequencing. It contains the first ATG (underlined) followed by several stop codons (red asterisk) in all reading frames. Also a large part the sequence coding for the proteoglycan-like domain (blue filled bars), that was originally interrupted by the PGK-neo cassette, was affected by the splicing modification. The RNA sequence coding for the CA domain (open green bar) was not affected by the splicing modification.

Whether the mutated transcript of *MN/CA9* gene has a coding capacity for a functional protein corresponding cDNA from *MN/CA9*$^{-/-}$ animals was analyzed in detail by 5'RACE using the gene specific primers. The sequence analysis of the resulting post-transcriptionally modified 5'end revealed a shortage of the mutated cDNA. The cDNA was by 280bp shorter on its 5' end. On the genomic level this 280bp fragment represents the first half of the exon 1 that was spliced out during the posttranscriptional modifications. On the protein level this

280bp fragment of the cDNA represents the signal peptide and a part of the proteoglycan-like domain that was deleted. The 5' end of the mutated cDNA was flanked by a short residue of the PGK-neo cassette that remained after the splicing modifications. It contained the first found ATG followed by multiple stop codons in all reading frames (Fig. 14). This result was confirmed by RT-PCR analysis of the 5' end of the cDNA. It was not possible to detect any PCR product by using the gene specific primers for the PGK-neo cassette and the murine *MN/CA9* cDNA (+1 - +280) (Fig. 15). The additional analysis of the *MN/CA9* cDNA 3' end (+281 - +1982bp) by RT-PCR from *MN/CA9*$^{-/-}$ animals was performed. In the region +281 - +1982bp no difference in the size of the cDNAs from *MN/CA9*$^{-/-}$ and *MN/CA9*$^{+/+}$ animals was found (Fig.15).

Together, the presence of stop-codons in all reading frames and the absence of the signal peptide indicates that the mutated transcript detected in the *MN/CA9*$^{-/-}$ mice is not functional.

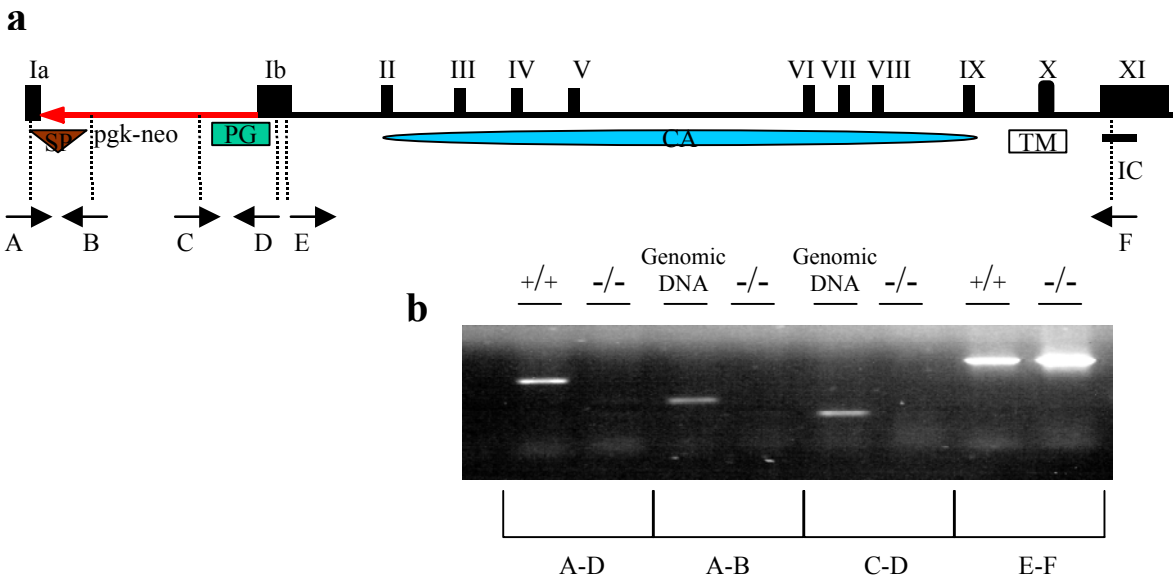

Fig. 15. (a) Schematic diagram of murine *MN/CA9* genomic structure (upper) and the MN/CA IX protein domains illustrating the impact of the mutation in *MN/CA9* gene detected by RT-PCR. The full boxes (I - XI) denote the exons; SP - signal peptide; PG - proteoglycan-like domain; CA - carbonic anhydrase domain; TM - transmembrane domain; IC - intracytoplasmic tail. The arrows show the direction and location of the gene specific primers (A, B, C, D, E, F). **(b)** Products detected by RT-PCR analysis of the RNA from stomach epithelium *MN/CA9*$^{-/-}$ and *MN/CA9*$^{+/+}$ mice. 1µg of total RNA from was used for reverse transcription and 3µl of the cDNA was subjected to PCR to determine the resulting mutation in the *MN/CA9*$^{-/-}$ mice. The position of gene specific primers (A-D; A-B; C-D; E-F) was as shown in **(a)**. As a control of amplification was used wild type RNA (A-D and E-F) or if PGK-neo gene specific primers were used genomic DNA from the *MN/CA9*$^{-/-}$ mice (A-B and C-D).

5.4. ANALYSIS OF THE MN/CA9 DEFICIENT MICE

5.4.1. Homozygous Mutant Animals Develop Normally and are Fertile

The heterozygous offspring of the germline transmitting chimeric mice had mixed 129/Ola x C57 BL/6J background. These mice were interbred and the genetic defect of *MN/CA9*$^{-/-}$ animals was analyzed in mice with 129/Ola x C57 BL/6J mixed background.

When heterozygous mice were interbred and the offspring genotyped at 3 weeks of age, the ratio was 1 : 2 : 1 corresponding to Mendelian rules. The males as well as the females from *MN/CA9*$^{-/-}$ animals were fertile, giving rise to an average of eight pups per litter. This result does not indicate embryonal lethality due to MN/CA IX deficiency even in *MN/CA9*$^{-/-}$ mating.

The birthweight and the postnatal growth of the *MN/CA9*$^{-/-}$ animals were normal as in the case of their wild type littermates. The appearance, behavior, health status and life span of 7-months-old *MN/CA9*$^{-/-}$ mice was indistinguishable from *MN/CA9*$^{+/-}$ and *MN/CA9*$^{+/+}$ mice. At present the oldest animals are 12 months old. So far, no statistically significant number of cases of early mortality was registered.

Age in months	Stomach hyperplasia	Inflammation in pancreas	Other phenotype
1	Yes	No	Liver, some inflammatory cells in the portal tract
2	Yes	Yes	No
2	Yes	Yes	Small intestine, mild adenomatous change
2 ½	Yes	Yes	Liver, some inflammatory cells in the portal tract
3	Yes	ND	ND
3	Yes	ND	Benign tumor of a sebaceous gland
4	Yes	ND	ND
5	Yes	No	Liver, mild fatty change
7	No	No	No
7 ½	Yes	No	Liver, mild fatty change and some inflammatory cells in the portal tract, small intestine, adenoma
8 ½	No	Yes	No
8 ½	No	Yes	Liver, large cysts, could represent massively enlarged portal veins
10 ½	Yes	No	No
11	Yes	No	Liver, mild fatty change
11 ½	Yes	No	Liver, mild fatty change
11 ½	Yes	Yes	Liver, fatty change
11	Intestestinal metaplasia	Yes	Lung, atypical epithelial cells in bronchioles

Tab. 7. Phenotypic changes registered in the *MN/CA9*$^{-/-}$ mice. ND - not done

5.4.2. Histological Examination of MN/CA IX *Mutant Mice*

All animals used for histological analysis were on mixed background. The tissue samples from lung, spleen, liver, kidney, pancreas, stomach, duodenum, jejunum, ileum and colon were examined in adult *MN/CA9*$^{-/-}$ and *MN/CA9*$^{+/+}$ mice. After hematoxylin-eosin (HE) staining the tissue sections were analyzed using light microscopy. No pathological changes were observed in lung, spleen, liver, kidney, jejunum, ileum and colon from the mutated animals when compared to those with wild type genotype.

The most remarkable abnormalities were found in the stomachs of 14 of 17 analyzed *MN/CA9*$^{-/-}$ mice. Additional pathological changes were seen in pancreas and duodenum (Table 6).

It is important to note that the mice heterozygous for MN/CA IX mutation were indistinguishable from their wild type littermates in histological analysis.

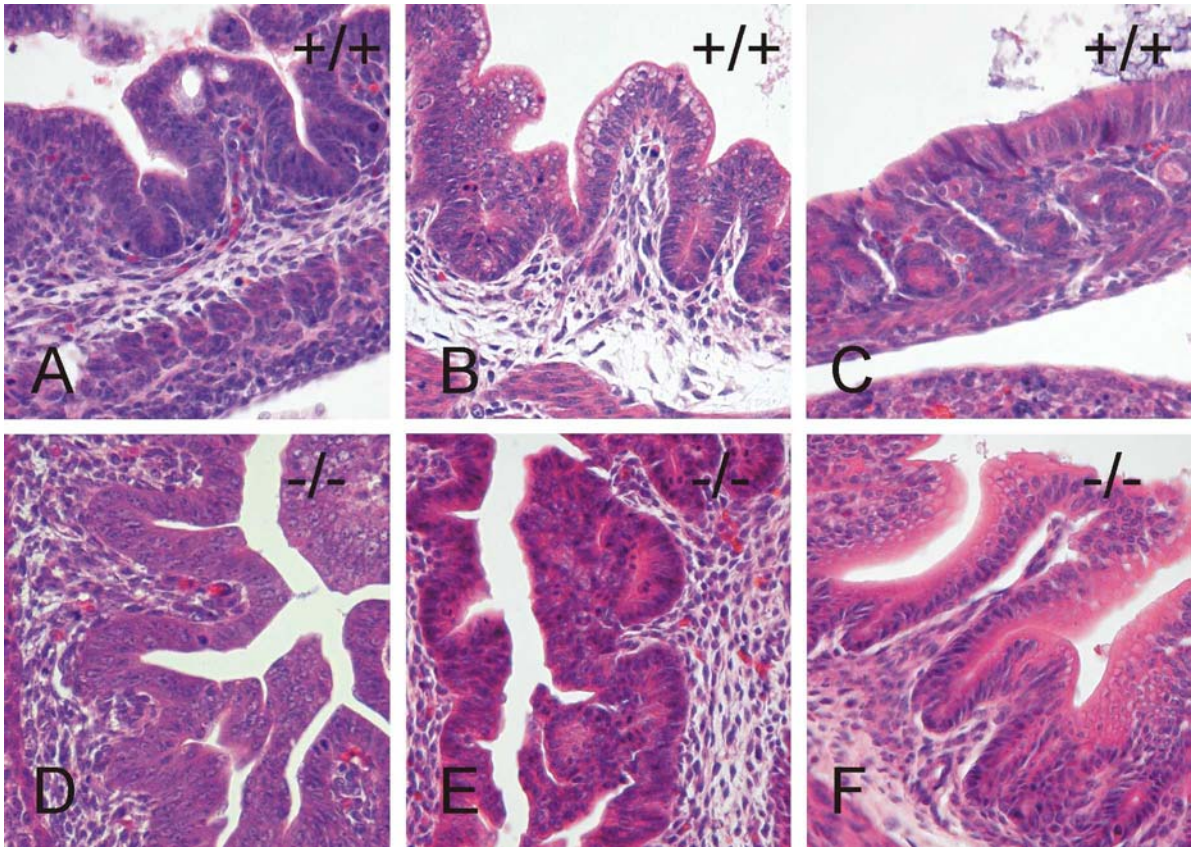

Fig. 16. Foetal development of the stomach in *MN/CA9*$^{+/+}$ and *MN/CA9*$^{-/-}$ mice. Paraffin sections from the embryos from wild type (A, B, C) or from mutant *MN/CA9*$^{-/-}$ (D, E, F) mice were stained with hematoxylin and eosin. The morphology of the gastric epithelium from the embryos of embryonal day E15,5 (A, D) and E17,5 (B, E) is in *MN/CA9*$^{+/+}$ and *MN/CA9*$^{-/-}$ mice normal. The stomach samples of the mice of postnatal day P0,5 (C, F) show first signs of the thickening of the developing gastric mucosa. (Magnification 400x).

5.4.3. Gastric Phenotype in MN/CA IX *Mutant Mice*

Histopathological examination of tissue samples from *MN/CA9*$^{-/-}$ mice showed major alteration in the stomach epithelium. Mutant *MN/CA9*$^{-/-}$ mice, their heterozygous and wild type littermates were investigated at different stages of development. In the group of mice sacrificed at day E15,5 and E17,5 no differences were seen between the stomachs of normal and *MN/CA9*$^{-/-}$ mice. The first changes were registered at postnatal day P0,5. At this stage of

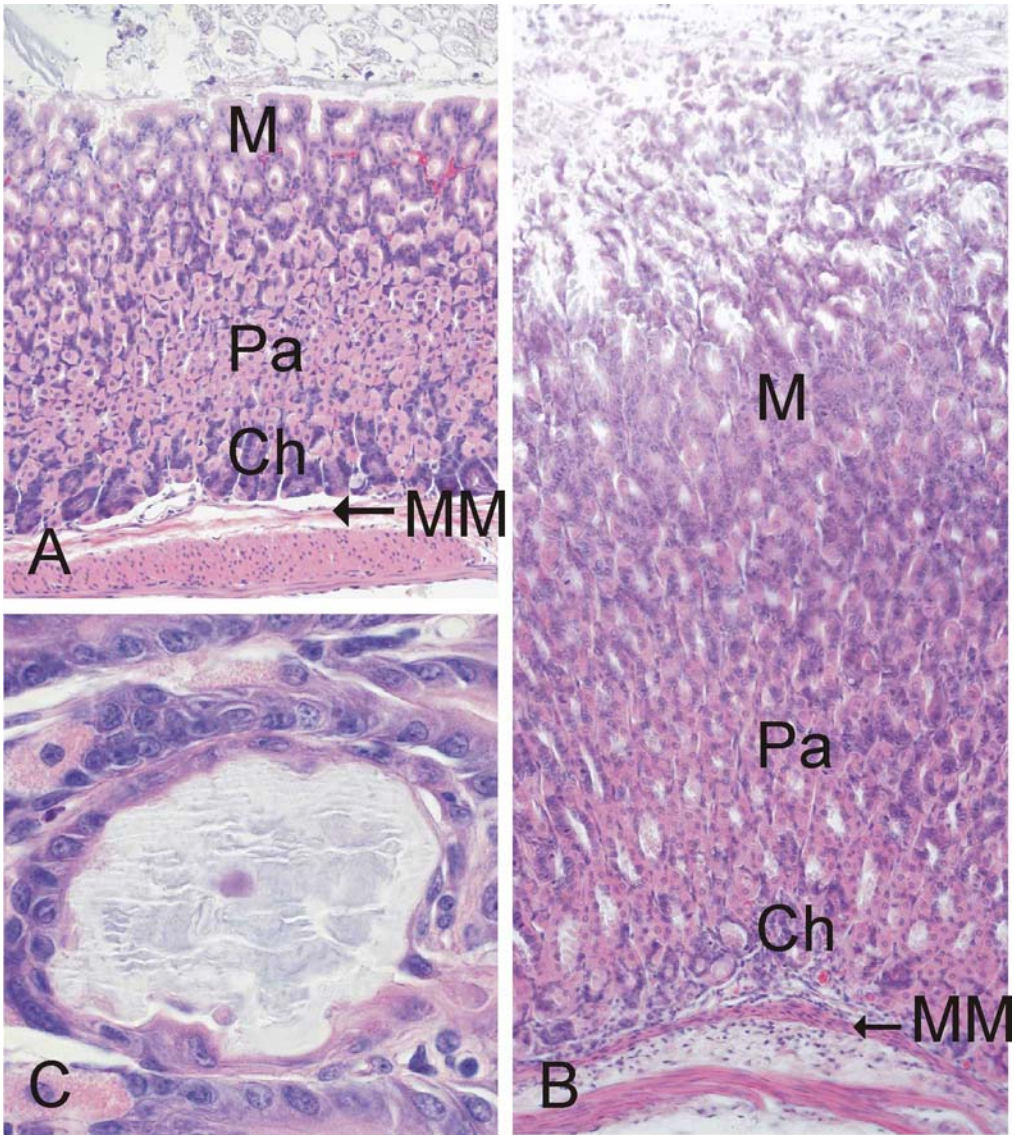

Fig. 17. Organization of the stomach mucosa in *MN/CA9*$^{+/+}$ **(A)** and *MN/CA9*$^{-/-}$ **(B)** mice. 5µm sections of stomach obtained from wild type **(A)** and mutant *MN/CA9*$^{-/-}$ **(B)** littermates were stained with hematoxylin and eosin. Note that the thickness of the gastric mucosa is greatly expanded in the adult *MN/CA9*$^{-/-}$ mouse (MM=muscularis mucosae; Ch=chief cells; Pa=parietal cells, M=mucus producing surface cells). The architecture of the epithelium in the *MN/CA9*$^{-/-}$ mouse is very much distorted. Large cystic changes in the stomach epithelium accompanied the perturbed stomach mucosa development of *MN/CA9*$^{-/-}$ mice **(C)**. (magnification **A, B** -200x; **C** -500x)

development, the gastric mucosa was slightly thicker in *MN/CA9*$^{-/-}$ mice when compared to the wild type littermates of the same age (Fig. 16).

The histological change became more apparent and clearly hyperplastic with age and was found to be prominent already in animals 1 month old. In some adult *MN/CA9*$^{-/-}$ mice, the morphologically abnormal gastric mucosa was as much as four-fold expanded, compared to the wild type controls (Fig. 17). In the wild type mice the pit-glands of the mucosa are orderly organized, while the histological architecture of *MN/CA9*$^{-/-}$ mice mucosa was severely distorted.

The hyperplasia affected both deep glandular epithelium and more superficial epithelium of the stomach (Fig. 17) while the squamous epithelium of the non-glandular region had a normal structure (not shown). Analysis of large specimens from several *MN/CA9*$^{-/-}$ mice indicated that the hyperplastic areas included all the major cell types of gastric epithelium: parietal cells, chief cells and the mucus secreting epithelial cells. This finding confirmed that cellular differentiation was apparently normal in spite of the null mutation in *MN/CA9*$^{-/-}$ protein. Normal structure of the subepithelial lamina propria was seen at all stages of development.

Despite the consistent finding of extensive gastric epithelial hyperplasia in *MN/CA9*$^{-/-}$ animals, no signs of dysplasia were observed in any of the studied sections of stomach.

In addition to the hyperplastic change, large pathological epithelial-lined cysts were seen in several *MN/CA9*$^{-/-}$ mice (Fig 17C). The content of the cysts remained mainly negative for Alcian blue, suggesting that they do not contain mucus.

5.4.4. Additional Changes in the Pancreas and the Intestine

Beyond gastric hyperplasia, 50% of comprehensively analyzed adult mutated animals showed mild or moderate accumulation of inflammatory cells in the pancreas (Tab. 7). The histological picture was indicative of chronic pancreatitis. Interestingly, pancreatic acinar cells showed strong MN/CA IX-positive staining at day E15,5 and E17,5 (data not shown). At this stage of development, MN/CA IX expression was very weak in other organs of the alimentary tract.

Moreover, small intestinal adenomas were observed in three of 15 *MN/CA9*$^{-/-}$ mice. One of them showed moderate dysplasia while the others showed only slight dysplasia (Tab. 7). The appearance of adenomatous changes could be associated with the absence of MN/CA IX protein, because it is normally highly expressed in the proximal small intestine.

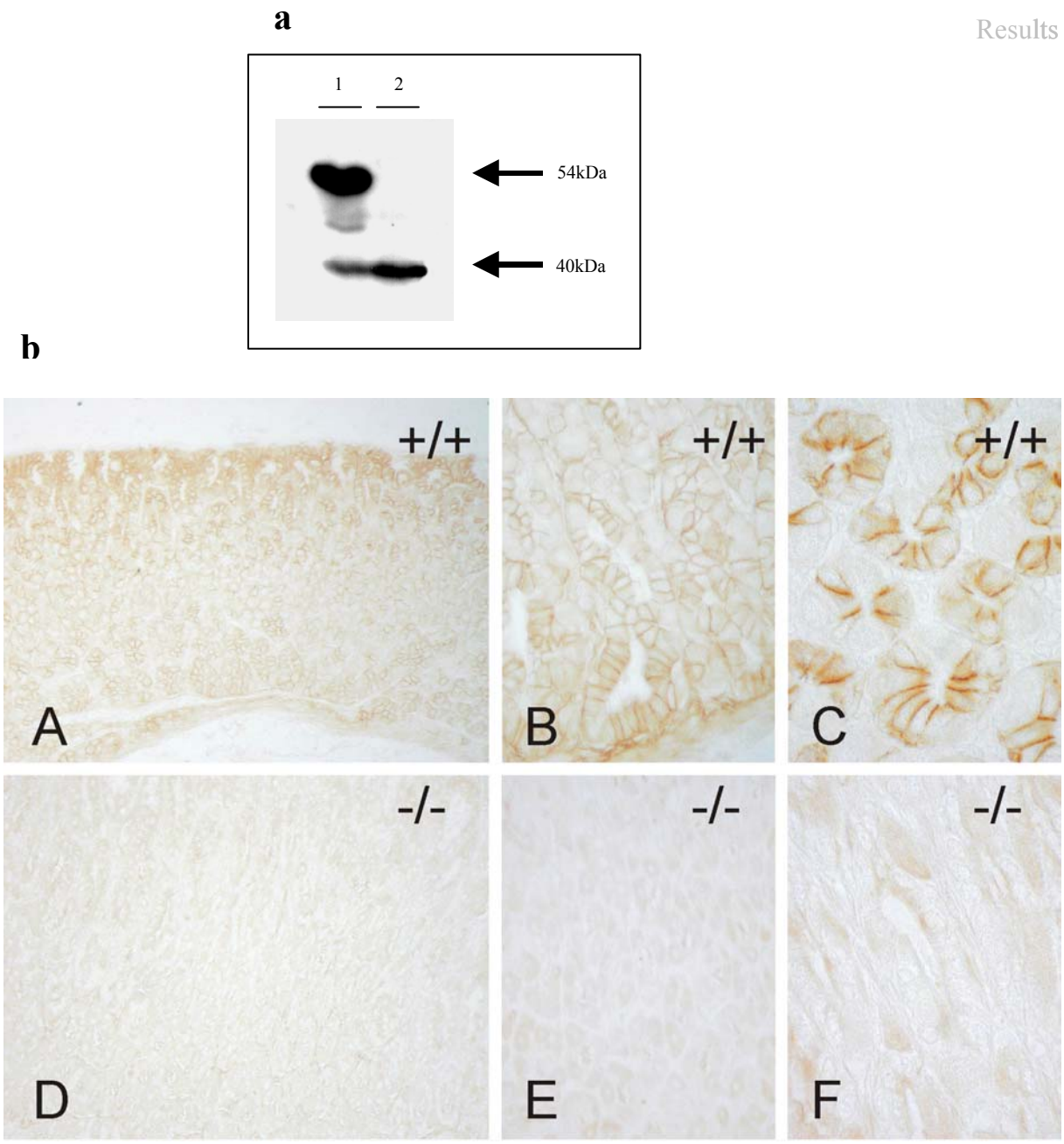

Fig. 18. (a) Western blot analysis of the protein extract of the *MN/CA9*$^{+/+}$ (lane 1) and *MN/CA9*$^{-/-}$ (lane 2) mouse stomach epithelium. Blots were reacted with anti-PG-MN rabbit antiserum raised against a synthetic peptide from the proteoglycan-like domain of MN/CA IX. The upper arrow points at the 54-kDa polypeptide of MN/CA IX. The 40-kDa polypeptide (lower arrow) represents an unknown protein recognized by this antibody. **(b)** Immunohistochemical staining of MN/CA IX in stomach sections obtained from the *MN/CA9*$^{+/+}$ (A, B, C) and *MN/CA9*$^{-/-}$ (D, E, F) mice. Panels A-C show strong positive staining in the gastric mucosa of wild type mice, especially in the mature glandular cells and the pit cells (A). The staining is located on the basolateral membrane of the cells (B, C). No positive staining was detected in the stomach of *MN/CA9*$^{-/-}$ mice (D-F). (Magnification A, D-200x; B, E-400x; C, F-500x).

5.4.5. Immunohistochemical Analysis of the MN/CA9$^{-/-}$ *and MN/CA9*$^{+/+}$ *Mouse Stomach Sections*

Immunohistochemical staining of the tissue sections obtained from both *MN/CA9*$^{-/-}$ and *MN/CA9*$^{+/+}$ mice was performed to explore the possible mechanisms that lead to gastric hyperplasia in the *MN/CA9*$^{-/-}$ mice. The expression of the MN/CA IX in the wild type and

MN/CA9$^{-/-}$ mouse stomach was investigated with anti-PG-MN antibody that recognizes murine MN/CA IX protein (Fig. 18 and 19). In the Western blot analysis, the specific MN/CA IX band was detected only in the protein extract from the wild type animals, while the protein extract from the mutant homozygotes remained unlabeled (Fig. 18a).

The immunohistochemical staining of the *MN/CA9*$^{+/+}$ mice stomach showed very strong signal in the mucosa. Strongest staining was detected in mature glandular and superficial epithelial cells with localization on the basolateral membrane (Fig 18b). The stomach from the *MN/CA9*$^{-/-}$ animals did not reveal any positive staining (Fig. 18b). While the positive staining in the *MN/CA9*$^{+/+}$ mice was confined to all epithelial cells of the corpus, the squamous epithelium of the forestomach turned out to be negative for MN/CA IX (Fig. 19). This explains the absence of any phenotypic changes in the forestomach of *MN/CA9*$^{-/-}$ mice.

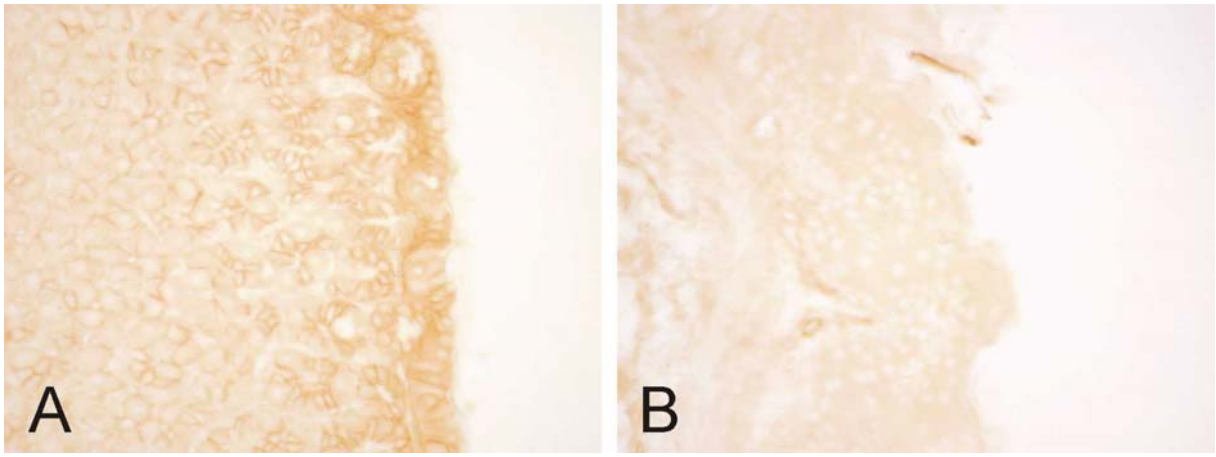

Fig. 19. Immunohistological staining of the wild type mouse stomach with the rabbit anti-PG-MN serum. **(A)** The columnar epithelium in the body of the stomach is positively stained, especially in the mature glandular cell region and the pit cell region. **(B)** The squamous epithelium of the forestomach remained negative. (Magnification 400x).

Since MN/CA IX has been linked to the regulation of cell proliferation (Saarnio *et al.*, 1998b), the expression of PCNA as a marker of proliferating cells was studied (Fig. 20). The pattern of PCNA expression was very different in mutated and wild type mice. Normal mice showed characteristic staining restricted to the proliferative zone of the gastric mucosa. In contrast, the hyperplastic gastric mucosa of *MN/CA9*$^{-/-}$ mice showed much more widely spread staining and the total number of PCNA-positive cells was markedly increased. However, counting of PCNA-positive cells in the distorted proliferative zone of the *MN/CA9*$^{-/-}$ mice revealed that the ratio between the number of proliferative cells and total number of cells in the proliferative area is approximately the same as in the wild type

control. No change in proliferative activity assessed by PCNA staining was observed in other gastrointestinal tissues (data not shown).

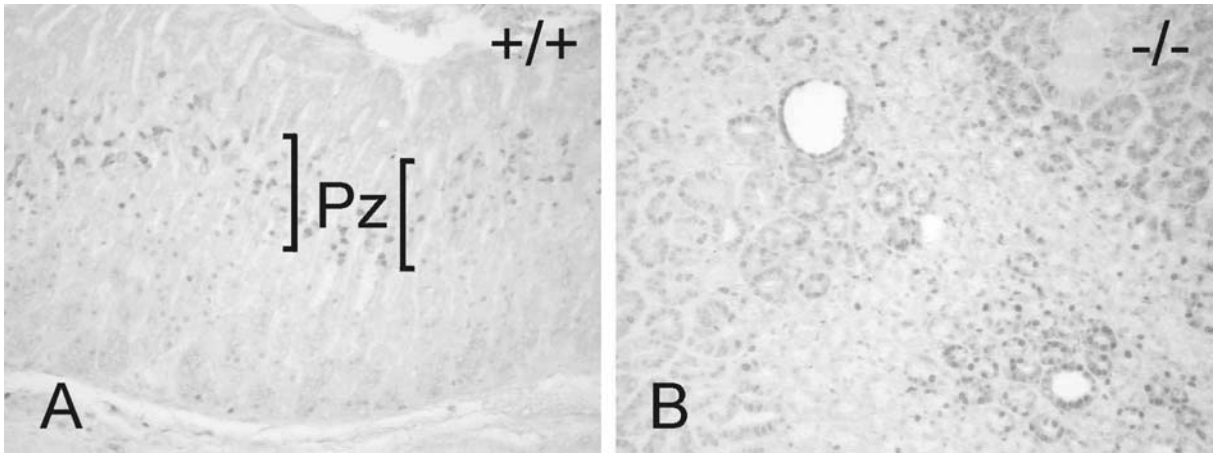

Fig. 20. The stomach epithelium of *MN/CA9*$^{-/-}$ mice exhibits disorganized immunostaining by PCNA antibody. The proliferative zone (Pz) in the wild type mice **(A)** is confined to the isthmus of the gland where the epithelial cells are clearly positive for PCNA. In the *MN/CA9*$^{-/-}$ mice **(B)** the proliferative zone is grossly enlarged and highly disorganized. (Magnification 200x).

In order to determine whether the increased amount of cells in the gastric epithelium of the *MN/CA9*$^{-/-}$ mice could be attributed to a defect in cellular death, the cells undergoing apoptosis were identified by extension of nicks in the DNA mediated by dUTP (TUNEL analysis). No differences in the ratio of number of apoptotic cells and non-apoptotic cells between the gastric mucosa from *MN/CA9*$^{-/-}$ and *MN/CA9*$^{+/+}$ mice were observed (data not shown).

Because MN/CA IX has recently been shown to participate in cell adhesion via its proteoglycan domain (Zavada *et al.*, 2000), the immunohistochemical analyses were extended to include some of the molecules, which are involved in adhesion mechanisms. High expression of MN/CA IX on the basolateral surfaces of the normal gastric epithelial cells also suggests a role in epithelial cell contacts (Pastorekova *et al.*, 1997). Immunohistochemical staining of E-cadherin in the samples from gastric mucosa of *MN/CA9*$^{-/-}$ and wild type mice is shown in figure 21. In the normal mice, E-cadherin showed strong positive staining in the mature epithelial cells locating both in the deep glands and the superficial part of the mucosa. In contrast, E-cadherin-positive staining was disorganized and slightly weaker in the hyperplastic mucosa of *MN/CA9* deficient mice. This slight difference in the staining intensity could not be confirmed by Western blot analysis, which revealed identical polypeptide bands for E-cadherin in both *MN/CA9*$^{-/-}$ and wild type mice (data not shown).

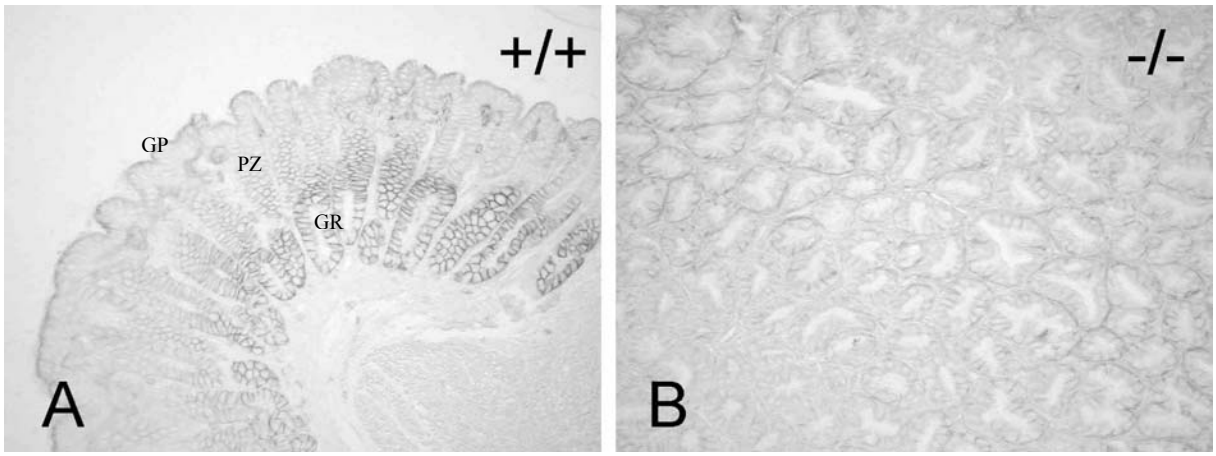

Fig. 21. Immunohistochemical staining of E-cadherin in stomach sections from the *MN/CA9*$^{+/+}$ **(A)** and *MN/CA9*$^{-/-}$ mice **(B)**. In the wild type mouse **(A)** the staining is localized in the gastric pit (GP) and the glandular region (GR), whereas the proliferative zone (PZ) shows much weaker signal. The mutated mouse **(B)** shows a disorganized staining pattern, reflecting the distorted architecture of the mucosa and the altered staining pattern for PCNA. Although the signal for E-cadherin is weaker, it is still present in the *MN/CA9*$^{-/-}$ mouse.

E-cadherin is linked to the actin cytoskeleton by the cytoplasmic catenins (Cowin and Burke, 1996). Furthermore β-catenin is involved in the wnt signaling pathway (Miller and Moon, 1996). α-Catenin and β-catenin were investigated by immunohistochemical staining. Both catenins showed strong positive immunoreaction in the gastric epithelial cells in both *MN/CA9*$^{+/+}$ and *MN/CA9*$^{-/-}$ mice. In the normal mice, the strongest signal was seen in the mucus secreting surface epithelial cells and fairly strong positive staining was also localized in the glandular cells. In the *MN/CA9*$^{-/-}$ mice, both catenins were widely expressed in the hyperplastic mucosa. Their distribution followed a similar disorganized fashion as described for E-cadherin (data not shown).

Together, the development of the gastric epithelium hyperplasia of *MN/CA9*$^{-/-}$ mice suggests that the regulation of cell proliferation is affected by the absence of the MN/CA IX protein in the stomach mucosa. Whether E-cadherin mediated cell adhesion is involved in these phenotypic changes of *MN/CA9*$^{-/-}$ mice remains still to be determined.

5.4.6. Systemic Acid-Base and Electrolytes Status

MN/CA IX protein is highly expressed in the epithelial cells of the gastric gland. As an enzymatically active carbonic anhydrase it might participate in the regulation of gastric acid-base homeostasis.

To determinate whether acid-base homeostasis in the homozygous mutant mice is altered, blood samples were taken from adult *MN/CA9*$^{+/+}$ and *MN/CA9*$^{-/-}$ mice. In plasma

electrolytes and blood pH measurements no differences were found. Also no differences were found in peptide hormone serum gastrin, known to play an important role in the regulation of acid secretion (Tab. 8).

Analysis of serum albumin showed slightly lower levels in the *MN/CA9*$^{-/-}$ mice in comparison to wild type littermates but the difference was not statistically significant.

Genotype	pH	HCO^{3-} (mM)	Cl^{-} (mM)	K^{+} (mM)	Na^{+} (mM)	Serum gastrin (pg/ml)
MN/CA9$^{+/+}$	7,30±0,035	24,35±1,95	119±2	3,8±0,6	139,5±4,5	60±4
MN/CA9$^{-/-}$	7,32±0,015	24,15±0,55	118±6	4,9±0,4	141,5±3,5	59±12

Tab.8. Plasma electrolytes, blood pH and serum gastrin were measured in two separate measurments from the blood of *MN/CA9*$^{+/+}$ and *MN/CA9*$^{-/-}$ animals.

5.5. CONCLUSIONS

In the present work three main goals have been reached. First, the murine *MN/CA9* cDNA and the genomic DNA were identified, cloned and characterized in detail. Second, a functional polyclonal antibody that can be used in Western blotting as well as in immunohistochemical analyses was prepared. Finally, a mouse with a null mutation in MN/CA IX protein was constructed in order to address basic questions of the physiological role of MN/CA IX in gastrointestinal tract and its possible function in oncogenesis. The results from the analysis of the *MN/CA9*$^{-/-}$ mice imply an important and non-redundant function of MN/CA IX protein in normal development of the stomach mucosa. It is likely that MN/CA IX protein, as an adhesion-like molecule, is involved in the regulation of signaling that leads to the cell proliferation of the gastric epithelium.